

Broken Symmetries and Kohn's Theorem in Graphene Cyclotron ResonanceJordan Pack¹,* B. Jordan Russell¹,* Yashika Kapoor¹, Jesse Balgley¹, and Jeffrey Ahlers¹*Department of Physics, Washington University in St. Louis,
1 Brookings Drive, St. Louis, Missouri 63130, USA*

Takashi Taniguchi

*International Center for Materials Nanoarchitectonics, National Institute for Materials Science,
1-1 Namiki, Tsukuba 305-0044, Japan*

Kenji Watanabe

*Research Center for Functional Materials, National Institute for Materials Science,
1-1 Namiki, Tsukuba 305-0044, Japan*Erik A. Henriksen¹†*Department of Physics, Washington University in St. Louis,
1 Brookings Drive, St. Louis, Missouri 63130, USA
and Institute for Materials Science & Engineering, Washington University in St. Louis,
1 Brookings Drive, St. Louis, Missouri 63130, USA* (Received 23 January 2020; revised 9 July 2020; accepted 18 August 2020; published 8 October 2020)

The cyclotron resonance of monolayer graphene, encapsulated in hexagonal boron nitride and with a graphite backgate, is explored via infrared transmission magnetospectroscopy as a function of the filling factor at fixed magnetic fields. The impact of many-particle interactions in the regime of broken spin and valley symmetries is observed spectroscopically. As the occupancy of the zeroth Landau level is increased from half-filling, a nonmonotonic progression of multiple cyclotron resonance peaks is seen for several interband transitions, revealing the evolution of underlying many-particle-enhanced gaps. Analysis of the peak energies shows significant exchange enhancements of spin gaps both at and below the Fermi energy, a strong filling-factor dependence of the substrate-induced Dirac mass, and also the smallest particle-hole asymmetry reported to date in graphene cyclotron resonance.

DOI: [10.1103/PhysRevX.10.041006](https://doi.org/10.1103/PhysRevX.10.041006)

Subject Areas: Graphene

I. INTRODUCTION

In graphene, Coulomb interactions combine with spin and valley degrees of freedom to generate an approximate SU(4) symmetry, which when broken can give rise to novel magnetic ground states in the quantum Hall regime at high magnetic fields. These phenomena have been explored by a variety of experimental probes, including electronic transport, quantum capacitance, and scanning probe microscopy experiments [1–7]. However, the excited states of this system due to collective excitations between Landau levels (LLs) in the broken-symmetry regime have not been

explored much to date [8,9]. Graphene is an ideal platform in which to pursue such studies because, in contrast to traditional two-dimensional electron systems having a parabolic dispersion, the linear dispersion of graphene allows the contribution of many-particle interactions to directly modify the LL transition energies in measurements of the cyclotron resonance (CR). Thus, the interplay of interaction effects and broken symmetries can be explored spectroscopically and on an even footing.

In this work, we study the CR in high-quality monolayer graphene by varying the LL filling factor at various fixed values of the magnetic field. Several interband transitions are observed to display nontrivial dependence on the filling factor. In the lowest interband transition, an intriguing pattern of resonances appears, starting with a single peak at half-filling of the $n = 0$ LL (ZLL), which then splits into four peaks at 3/4-filling and reduces to just two as the level becomes completely occupied; meanwhile, the higher interband excitations show interesting sequences of spectral weight shifts with the changing LL occupation. Using a

* J. P. and B. J. R. contributed equally to this work.

† henriksen@wustl.edu

Published by the American Physical Society under the terms of the Creative Commons Attribution 4.0 International license. Further distribution of this work must maintain attribution to the author(s) and the published article's title, journal citation, and DOI.

simple model of transitions between LLs having interaction-enhanced valley and Zeeman gaps, we find that the gap in the ZLL arising from coupling of graphene to the encompassing hexagonal boron nitride (hBN) becomes strongly enhanced both at half-filling and as the magnetic field is increased. Moreover, we observe an enhancement of Zeeman gaps both at and well below the Fermi level, with the latter indicating an indirect exchange coupling due to lattice-scale interactions coupling the two valleys in graphene. While this work specifically addresses physics in graphene, the approach is applicable, in principle, to any system with a linear dispersion and thus may find utility in understanding the competing roles of interactions and symmetry breaking in Dirac, Weyl, or strongly correlated materials [10,11].

In a strong magnetic field and absent symmetry breaking, graphene develops fourfold degenerate LLs (two each for electron spin and the K and K' valleys) with single-particle energies given by $E_n = s_n \hbar \omega_c \sqrt{|n|}$, where $\omega_c = \sqrt{2} v l_B^{-1}$ is the cyclotron frequency, $v \sim 10^6$ m/s is the band velocity, $l_B = \sqrt{\hbar/eB}$ the magnetic length, $s_n = \text{sign}(n)$, and $n = 0, \pm 1, \pm 2, \dots$ is the orbital index [12,13]. If the sublattice symmetry of graphene is broken, as is common for hBN-encapsulated devices, the valley-polarized $n = 0$ level is split by $E_{0,K}(E_{0,K'}) = +(-)M$, where M is the Dirac mass [14], and the $|n| > 0$ levels are shifted according to $E_n = s_n \hbar \omega_c \sqrt{|n| + \mu^2}$, with $\mu = M/\hbar \omega_c$. The CR energies of interband or intraband transitions from LL m to n are then given by the level separation

$$\Delta E_{m,n} = \hbar \omega_c \left(s_n \sqrt{|n| + \mu^2} - s_m \sqrt{|m| + \mu^2} \right), \quad (1)$$

with the selection rule $|n| - |m| = \pm 1$. In graphene, these energies can also include contributions from many-particle interactions, in contrast to materials with a parabolic dispersion where the center-of-mass and interparticle coordinates are separable and CR becomes insensitive to electron interactions, a result known as Kohn's theorem [15–17]. The linear dispersion of graphene mixes these coordinates so that interactions can directly impact LL transitions [18–23], leading to deviations from Eq. (1) [8,24–27] and a dependence of CR on the LL filling factor, $\nu = 2\pi n_s l_B^2$, where n_s is the charge carrier sheet density [28].

The sample used in this study is an $820\text{-}\mu\text{m}^2$ sheet of monolayer graphene sandwiched between approximately 40-nm-thick flakes of hexagonal boron nitride, assembled using a dry-stacking technique [29] and placed on a 4-nm-thick flake of single-crystal graphite lying on a lightly doped, oxidized Si wafer. Electrical contacts to the edge of the graphene were made using 3/60-nm-thick films of Cr/Au, defined by standard electron beam lithography fabrication. A 90- μm aluminum foil aperture restricts the infrared light to the region immediately surrounding the

sample. All spectroscopic data in this work were acquired at a base temperature of 300 mK (estimated sample temperature of less than 2 K [30]) for fixed values of the magnetic field using a broadband Fourier-transform infrared spectrometer with instrumental resolution of 0.5 meV (with exploratory traces at other resolutions [30]). Unpolarized blackbody light from the spectrometer was coupled through a KBr window into a cryogen-free dilution refrigerator with a 14-T solenoid, focused to and defocused from the sample using custom parabolic optics, and funneled via a compound parabolic collector to a composite Si bolometer. Traces are acquired at target LL filling factors and normalized to spectra taken at much higher ν , where many of the transitions at the target ν are Pauli-blocked, so that absorption features common to both traces divide to unity [30]. Each normalized spectrum was averaged for approximately 4 h.

II. CYCLOTRON RESONANCE RESULTS

A. Overview

In graphene, several interband CR transitions T_i can be observed simultaneously at fixed filling factor, comprising nominally degenerate pairs of inter-LL excitations $n = -i \rightarrow i - 1$ and $1 - i \rightarrow i$ with energies given by Eq. (1). Figure 1(a) shows a color map of transitions T_1 through T_5 acquired as a function of ν , in which the square-root dependence of the energies on the LL indices is immediately apparent. A schematic of the allowed transitions at half-filling is drawn in Fig. 1(b), and a representative line cut at $\nu = 0$ is shown in Fig. 1(c). The very narrow resonances follow from recent improvements in sample fabrication [31,32] and are key to enabling our observations. In Fig. 1(d), we show T_1 at $\nu = 0$ in devices from the present and two prior works [25,28], revealing a clear decrease in the half width at half maximum, Γ . In fact, the lower two traces in Fig. 1(d) provide a comparison of two common gating methods: The middle trace is acquired in a sample with a distant, doped Si/SiO₂ substrate on which the encapsulated monolayer rests [28], while the lower trace from the present work uses a local graphite gate. By chance, these two devices have similar charge carrier mobilities of 200 000 cm²/Vs, but the graphite-gated device shows greater values of the quantum scattering time τ_q extracted from Shubnikov–de Haas oscillations [33], reflecting improved screening of charged impurities in the SiO₂ by the graphite. The CR lifetimes $\tau_{\text{CR}} = \hbar/\Gamma$ in Fig. 1(e) are similarly improved, and in fact, the value of about 600 fs quoted for the present device is a lower limit, as even narrower lines with $\tau_{\text{CR}} \approx 2.5$ ps ($\Gamma = 0.26$ meV) are seen at higher instrumental resolution. This latter value is close to the transport time derived from the mobility [30], suggesting that impurity collisions limit the CR lifetime. Consistent with prior observations of CR in AlGaIn/GaN heterostructures [34], τ_{CR} can be several times larger than

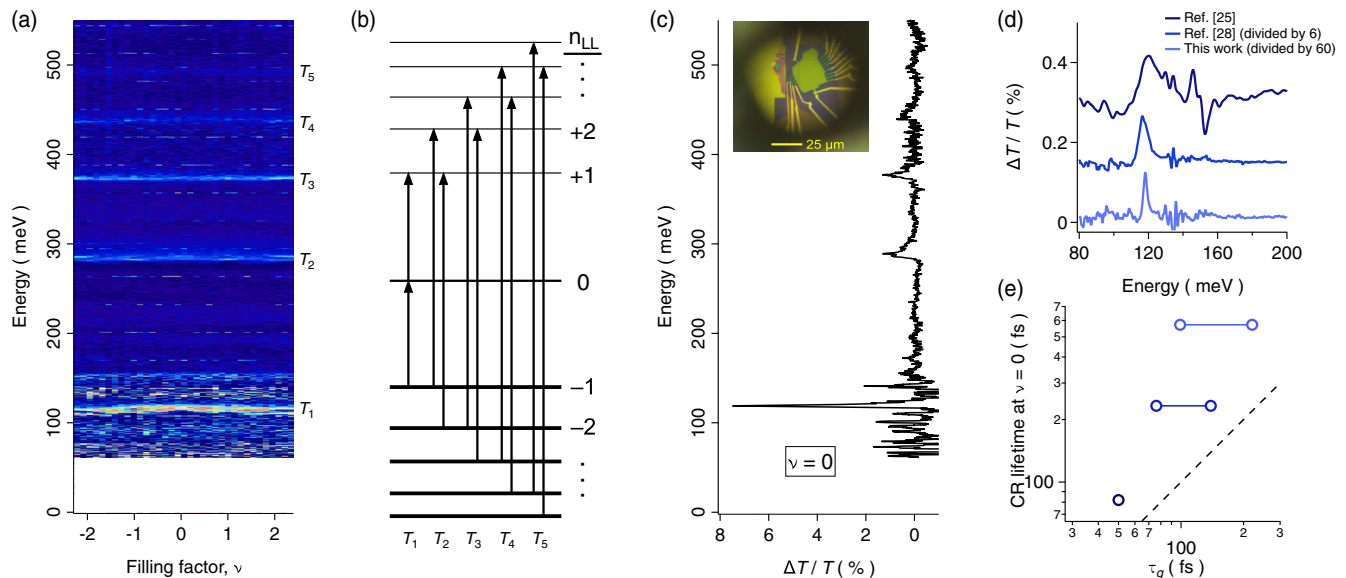


FIG. 1. Cyclotron resonance transitions in graphite-gated monolayer graphene at $B = 8$ T. (a) Color map of the normalized transmission spectra $\Delta T/T$ in the midinfrared as a function of the LL filling factor ν , measured in the device shown in the inset to panel (c). Several sharp CR transitions are visible, labeled T_1 through T_5 . The higher noise in the region of T_1 is due to the overall lower transmission in the 60–150-meV energy range, compared to the other transitions (and below 60 meV, the signal goes to zero) [30]. (b) Schematic showing the allowed Landau-level transitions at $\nu = 0$, consisting of nominally degenerate pairs. (c) Representative line cut of the color map at $\nu = 0$. (d) Evolution of CR line shape at $\nu = 0$ with the sample quality: The top trace is from a graphene-on-SiO₂ device with mobility of 17 000 cm²/Vs [25], the middle is from a hBN-encapsulated device on SiO₂ [28], and the bottom is the present graphite-gated, hBN-encapsulated device; the latter two have the same mobility, $\mu \approx 200\,000$ cm²/Vs. (e) CR lifetime $\tau_{\text{CR}} = \hbar/\Gamma$ at $\nu = 0$ (Γ is the half width at half maximum) vs a spread of quantum scattering times τ_q , derived from Shubnikov–de Haas oscillations acquired for a range of carrier densities at 3 K [colors correspond to traces (d)] [30]. The dashed line marks $\tau_{\text{CR}} = \tau_q$.

τ_q , which is reduced by variations in the carrier density across the sample.

B. Filling-factor dependence of T_1

In Fig. 2, we focus on the T_1 transition over filling factors $\nu = 0$ to $+6$, where a marked nonmonotonic evolution is seen from a single resonance at $\nu = 0$, to four resonances around $\nu = +1$, which reduce back to two for $\nu \gtrsim +2$, which both fade away as $\nu \rightarrow 6$ and the $n = +1$ LL is completely filled; a sudden sharp rise in the lower-energy resonance above $\nu = 5$ presages the extinction of the resonance. Line cuts in Fig. 2(b) show details at half-integer ν . The resonances manifest in intriguing patterns: The higher-energy peaks at $\nu = 1$ appear and disappear at different ν values, while the lower-energy pair appear simultaneously and then merge with increasing ν . At $\nu = 2$, the upper peak first appears at a lower energy near $\nu = 3/2$ and then rapidly rises before leveling off for $\nu \gtrsim 2$. Note that these features at $\nu = 1$ and 2 persist over a wide range of ν . This effect is real and not due, for instance, to small variations in the carrier density across the sample: From the width of the Dirac peak in the zero-field resistance vs density, we estimate a distribution of carrier densities $\delta n_s \approx 2 \times 10^{10}$ cm⁻², or $\delta \nu \approx 0.1$ at 8 T, rather smaller than the range over which the $\nu = 1$ and 2 features persist [30].

At $\nu = 1/2$ and $3/2$, broad resonances appear that, nevertheless, maintain the full spectral weight, suggesting all transitions are present but undifferentiated [30]. This could indicate the presence of dark magnetoexciton modes serving as additional scattering channels: There are up to 16 distinct transitions between the 0 and ± 1 LLs, although only the four that conserve the spin and valley are optically active [18].

In Fig. 2(c), we introduce schematics representing the simplest model of transitions between the $n = 0$ and ± 1 LLs that aligns with the observed CR. These schematics are drawn for $\nu = 0, +1$, and $+2$, with each of the four spin and valley levels shown explicitly, albeit with greatly exaggerated level shifts and gap sizes. In graphene, the inapplicability of Kohn's theorem implies the CR transition energies will reflect the single-particle LL separations plus many-particle shifts of the levels, along with excitonic and exchange corrections due to the excited electron and remnant hole [18–20,35,36]. Of course, the measured energies do not indicate which portion is due to level shifts vs exciton corrections. Therefore, we model each transition energy as a sum of the LL separation plus the difference of any valley and Zeeman gaps in each level, with the understanding that these gaps are meant to represent both single- and many-particle energies.

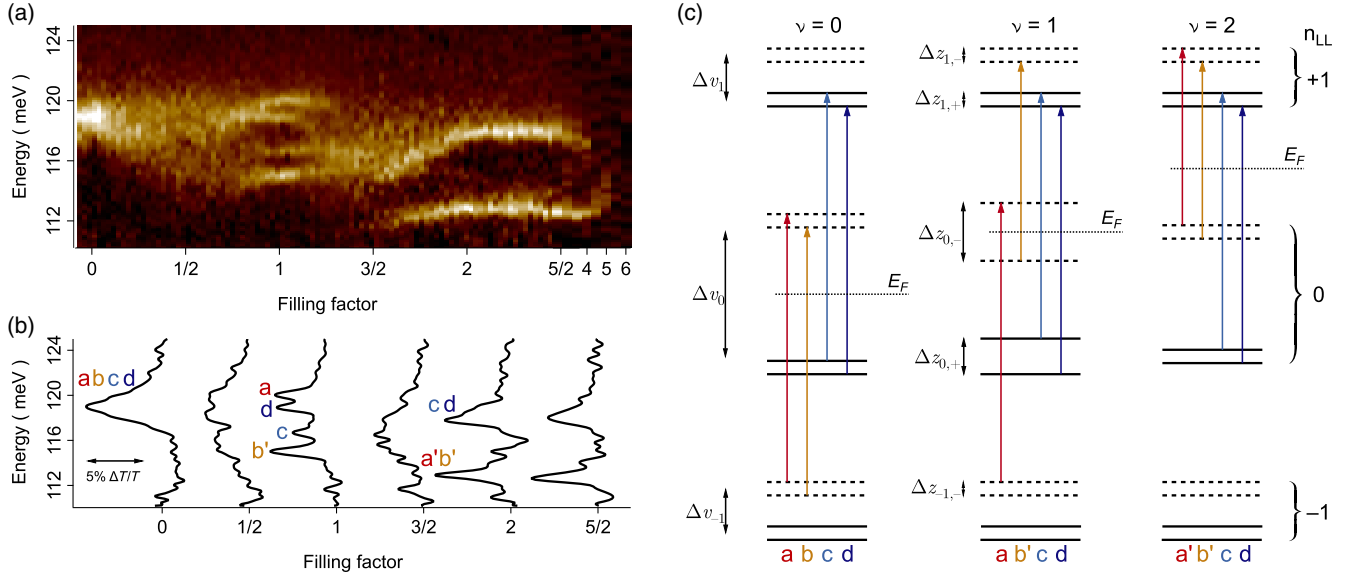


FIG. 2. Evolution of transition T_1 vs filling factor. (a) High-resolution map of T_1 vs filling factor from $\nu = -0.07$ to $\nu = +2.5$. Traces were acquired every $\delta\nu = 0.026$, with additional traces at $\nu = 3, 3.5, \dots, 6$. Starting with a single bright peak at $\nu = 0$, four peaks appear near $\nu = +1$, which reduce to two peaks at $\nu = 2$ and higher. By $\nu = 6$, the T_1 transition is extinguished as the participating LLs are filled. (b) Detail of transitions by line cuts at half-integer fillings. The linewidths at $\nu = +1$ are the narrowest observed, with τ_{CR} reaching 2.5 ps, or a resonance quality factor $Q = 220$. In between integer values of ν , only a single broad resonance is resolved. (c) Schematic of transitions involving the $n = -1, 0$, and $+1$ LLs. Solid (dashed) lines indicate the K (K') valleys, with valley gaps Δv_i and spin splittings Δz_i explicitly included. The Fermi energy E_F is shown as a dotted line. Each of the four spin and valley-preserving CR transitions are shown in different colors, corresponding to the labels a, b, c , and d . As the filling factor is increased, the two transitions from $n = -1$ to 0 become Pauli blocked and are replaced by transitions from $n = 0$ to $+1$; this is indicated by a label change $a, b \rightarrow a', b'$. Gaps indicated in this schematic represent single-particle levels enhanced by electron-electron interactions as discussed in the text.

For instance, at $\nu = +2$, two resonances are observed, although up to four transitions [two each for the valley and spin, labeled a', b', c , and d in Fig. 2(c)] are allowed. All LLs are either completely filled or empty, so interactions are expected to be minimized. If we assume that the Zeeman splittings in the $n = 0$ and 1 LLs are equal, then the observed CR splitting $\Delta E^{\nu=2} = E^{c,d} - E^{a',b'}$ arises from transitions originating on either side of the valley gap in $n = 0$. Note that if the $n = 1$ LL also has a nonzero valley gap, it is still the *difference* of these gaps, $\Delta v^{\nu=2} \equiv \Delta v_0 - \Delta v_1 = \Delta E^{\nu=2}$, that is detected. If the Zeeman splitting were also enhanced in one level over another, this picture would predict additional resonances that are not present in the data. Fitting the two peaks at $\nu = 2$ with Lorentzians, we find $\Delta E^{\nu=2} = 5.0(1)$ meV. Since any valley splitting of the $n = 1$ LL is likely to be small, this result should be a good measure of the valley gap in the ZLL. We identify this gap as due to sublattice symmetry breaking from the presence of hBN [5] and calculate a Dirac mass $M = 2.5$ meV.

At $\nu = 0$, the single peak indicates that the four allowed transitions are all degenerate. By the schematic in Fig. 2(c), the CR energy is given by the LL separation plus half the difference of the valley gaps in the zeroth and ± 1 LLs. That a single resonance is seen implies the valley gaps in the

$n = \pm 1$ levels must be equal; in addition, all of the Zeeman gaps must be the same, or additional CR lines would be seen. Actually, the $\nu = 0$ resonance is the broadest in T_1 , suggesting there may be unresolved lines due either to a differential enhancement of these gaps or a level repulsion between the two degenerate pairs labeled $\{a, b\}$ and $\{c, d\}$ in the figure if lattice-scale interactions couple the K and K' valleys. Indeed, such a splitting appears at 13 T as discussed below. For now, we determine the valley-gap difference to be $\Delta v^{\nu=0} = 2(E^{\nu=0} - E_{\text{avg}}^{\nu=2}) = 7.3(5)$ meV, where $E_{\text{avg}}^{\nu=2}$ is the average energy of the two peaks at $\nu = 2$. This difference yields a Dirac mass of 3.7 meV, substantially enhanced over its value at $\nu = 2$.

Finally, four resonances are seen at $\nu = 1$, which requires each transition to comprise a unique combination of valley and spin gaps in the initial and final LLs. In Fig. 2(c), we sketch a scenario where, for instance, the two transitions $\{c, d\}$ (which are degenerate at $\nu = 0$ and $+2$) now gain distinct energies at $\nu = 1$ when the Zeeman gaps in the $n = 0$ and 1 LLs become unequal. Moreover, the two Zeeman gaps in the $n = 0$ level marked $\Delta z_{0,-}$ and $\Delta z_{0,+}$ must be differentially enhanced, or else the transitions marked a and d will remain degenerate. The difference of the valley-gap energies in the $n = 0$ and ± 1 LLs, namely, $\Delta v^{\nu=1} = \Delta v_0 - \Delta v_{\pm 1}$, and the two Zeeman differences

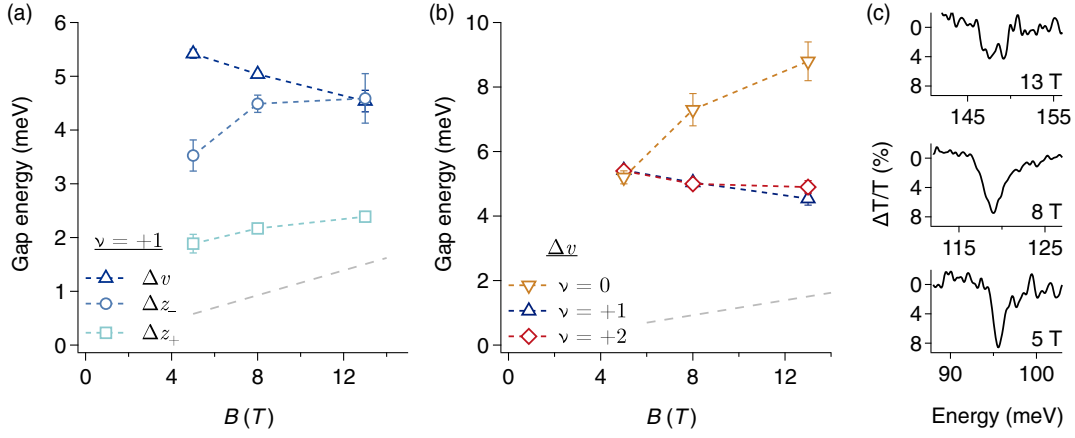


FIG. 3. Evolution of splittings with magnetic field. (a) Magnetic-field dependence of the observed gaps at $\nu = 1$. The valley gap Δv appears to decrease with increasing field, while the spin gaps Δz_- and Δz_+ increase with increasing field. All splittings observed are significantly larger than the bare Zeeman energy shown as a gray dashed line. (b) Comparison of the valley gaps calculated at integer filling as a function of magnetic field. (c) T_1 resonance at $\nu = 0$ for three magnetic fields. With increasing field, the resonance broadens and shows an incipient splitting.

$\Delta z_- = \Delta z_{0,-} - \Delta z_{\pm 1,-}$ and $\Delta z_+ = \Delta z_{0,+} - \Delta z_{1,+}$, can be extracted by inverting a matrix that records the contribution of each gap to the transition energy. The full procedure is described in the Supplemental Material [30] and yields $\Delta v^{\nu=1} = 5.0$ meV, $\Delta z_+ = 2.1$ meV, and $\Delta z_- = 4.3$ meV. Note we assume that gaps in the $n = \pm 1$ levels are identical. While the size of this valley gap is close to that found at $\nu = +2$, the spin gaps are significantly larger than the bare Zeeman energy at this field, $E_Z = 0.93$ meV, indicating a clear role for electron interactions. The enhanced Δz_+ splitting is notable, as both levels are occupied and well below the Fermi energy. This case is reminiscent of indirect exchange splitting in the spin sector seen in GaAs quantum wells [37], except that here the splittings occur in different valleys, indicating the presence of lattice-scale interactions coupling valleys K and K' . Meanwhile, the size of Δz_- at the Fermi energy compares well to a transport gap of about 5 meV, for $\nu = -1$ at 9 T, as found in Ref. [4]. Casting these as effective g factors, we find the spin gap at the Fermi level has $g_{z,-}^* = \Delta z_- / \mu_B B = 9.3$, and the buried spin gap (in the K valley) has $g_{z,+}^* = 4.5$.

We briefly note that although Kohn's theorem does not hold in graphene, in general, a limited version is predicted to survive for the T_1 transition [18–20]. However, the filling-factor-dependent shifts and splittings found here strongly imply that even this remnant does not hold. We speculate that either the hBN-induced moiré pattern (with a length scale comparable to the magnetic length) or the lattice-scale interactions invoked to explain the $\nu = 0$ ground state [6] are sufficient to break translation invariance and render Kohn's theorem inoperable.

C. Magnetic-field dependence of T_1

To better understand the nature of these splittings, we show the magnetic-field dependence of the extracted spin

and valley gaps at $\nu = 1$ in Fig. 3(a). The measured spin-gap energies are substantially larger than the Zeeman energy, which suggests an interaction enhancement consistent with the ferromagnetic ground state at quarter-filling in Ref. [4]. The gaps exhibit a sublinear increase with magnetic field, close to the \sqrt{B} dependence expected for interaction effects, although further work is needed to understand the precise field dependence. Unlike the spin gaps, the $\nu = 1$ valley gap is observed to decrease with increasing magnetic field. In Fig. 3(b), this valley gap is compared with those for the half-filled and fully filled $n = 0$ LL, where we find the gaps at $\nu = 1$ and 2 remain closely matched as the field changes. Since interaction effects should be weakest at $\nu = 2$, this agreement suggests the valley gap at $\nu = 1$ is hardly impacted by interactions. In contrast, the valley gap extracted for $\nu = 0$ increases dramatically with increasing magnetic field, consistent with the understanding that the ground state at $\nu = 0$ involves an interaction-driven breaking of valley symmetry, which drives an enhancement of the gap [4,6,38]. A closer look at $T_1(\nu = 0)$ for multiple fields in Fig. 3(c) shows the resonance broadens at 8 T compared to 5 T, and it develops a clear splitting by 13 T [note $\Delta v^{\nu=0}$ in Fig. 3(b) uses the average value of this splitting]. As noted previously, this result is perhaps due to level repulsion of degenerate transitions in the two valleys by short-ranged Coulomb interactions, known to be important in the study of graphene and quantum Hall ferromagnetism but not yet studied in the context of CR in graphene [38,39].

D. Particle-hole asymmetry

In Fig. 4(a), we zoom out to show T_1 over an equal range of positive and negative filling factors and find a small but clear particle-hole asymmetry. For example, while the $\nu = \pm 2$ splittings are virtually identical in size at 5.0 meV, the hole-side peaks lie a full 1.0 meV lower in energy.

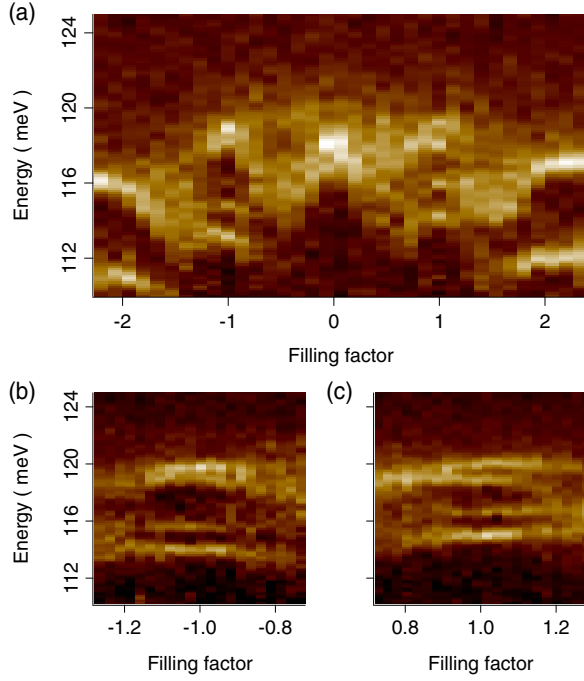


FIG. 4. Particle-hole asymmetry. (a) Close-up of T_1 transition from Fig. 1(a), showing a clear asymmetry for positive vs negative filling factors. (b,c) Higher-resolution (finer abscissa spacing) maps at $\nu = -1$ and $+1$, respectively, revealing particle-hole symmetry breaking in the fourfold splittings.

Moreover, a closer look at $\nu = -1$ and $+1$ in Figs. 4(b) and 4(c) shows that the two lower-energy transitions are both separated by 1.7 meV and exhibit a slow increase with increasing $|\nu|$, but the hole-side pair is found to be 1.1 meV lower than the electron-side pair. Meanwhile, the two higher-energy peaks on the hole side nearly overlap, compared to $\nu = +1$, where we have seen that they are individually resolved. Additionally, the relative shift of

these higher-energy peaks with increasing $|\nu|$ shows opposing trends near $\nu = -1$ and $+1$, with both pairs lying close together at the left side of the graphs (more negative ν) and separating toward the right (for more positive ν), breaking $\nu \rightarrow -\nu$ symmetry. Finally, the highest energy peak on the hole side is only 0.4 meV lower than the electron side. Relative to the CR energy, this symmetry breaking is a nearly 0.8% effect, too small to have been noticed in early broadband spectroscopic studies [24] but matching an asymmetry apparent in the data of Refs. [25,28]. However, in terms of the many-particle-enhanced valley and spin gaps, these small shifts are quite significant. For instance, applying the same analysis used in the discussion of Fig. 2, we find for $B = 8$ T that $\Delta v^{\nu=-1} = 5.7$ meV, $\Delta z_+^{\nu=-1} = 1.2$ meV (or effective g factor $g_{z,+}^* = 2.6$), and $\Delta z_-^{\nu=-1} = 6.7$ meV ($g_{z,-}^* = 14.4$).

Such particle-hole asymmetry is not predicted by many-particle theories to date but may arise at the single-particle level due to next-nearest-neighbor hopping [40]. In this picture, a field-dependent asymmetry between the $-n \rightarrow n-1$ and $1-n \rightarrow n$ transitions was derived for the high- n limit in Ref. [41], giving $E_{\text{asym}} = 3\sqrt{2}\hbar\omega_c t'a / tl_B \approx 0.56$ meV at 8 T [where $t(t')$ is the nearest (next-nearest) neighbor hopping, and a the C-C atom distance in graphene]. This value lies within a factor of 2 of the asymmetry energies seen here, suggesting we are seeing an intrinsic property of the underlying band structure. In contrast, far larger particle-hole asymmetries up to a few percent of $E_{0,1}$ have been reported in swept-field CR studies of graphene-on-oxide, monolayer and multilayer epitaxial graphene, and encapsulated graphene with double moiré potentials [8,9,42,43].

E. Effective and renormalized band velocities

In Fig. 5(a), the transition energies at $\nu = 0$ and 8 T are plotted as a function of transition number T_i , parametrized as an effective velocity $v_{\text{eff}}(T_i) = \Delta E^{\text{meas}}(T_i) / \Delta E^{\text{calc}}(T_i)$

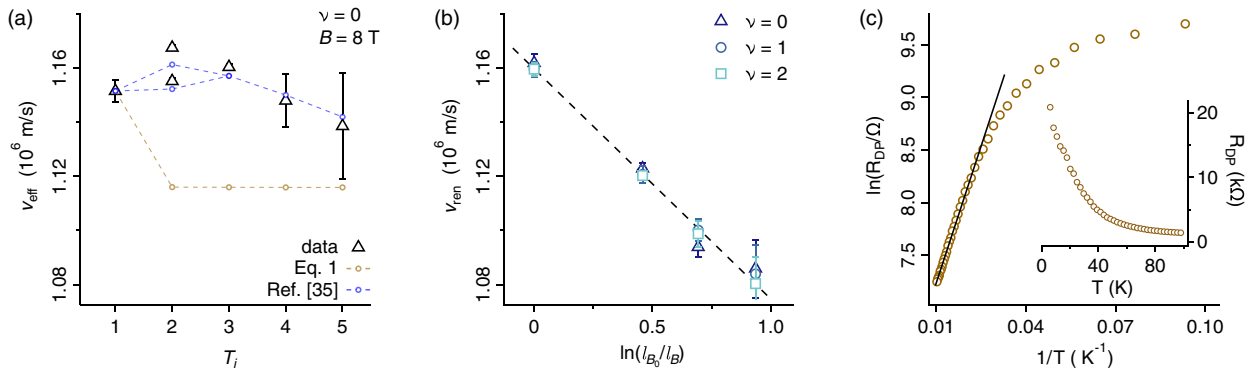


FIG. 5. Effective velocity, renormalized velocity, and activated transport. (a) Transition energies parametrized as effective velocities $v_{\text{eff}} = \Delta E^{\text{meas}}(T_i) / \Delta E^{\text{calc}}(T_i)$ [$v = 10^6$; $\mu = 0$] at $\nu = 0$. The dashed lines predict v_{eff} using two approaches: The tan lines show the single-particle model of Eq. (1) including a finite Dirac mass, while the blue lines are calculated using the many-particle theory of Ref. [35]. (b) Renormalized Fermi velocity v_{ren} , extracted from fits to the theory of Ref. [35], plotted vs the logarithm of \sqrt{B} . The resulting linear dependence is the magnetic-field equivalent of the zero-field velocity renormalization in graphene [20,22,46,47]. (c) Arrhenius plot of the device resistance at charge neutrality and zero magnetic field. The slope implies a gap of 15.0 meV. The inset shows the measured resistance vs temperature.

$[v = 10^6; \mu = 0]$. We see that v_{eff} increases from T_1 to T_2 and, thereafter, gradually decreases in agreement with previous measurements [28]. We fit these data in two ways: First, in the basic noninteracting picture with energies given by Eq. (1), using fixed band velocity v and mass μ (with μ set equal to the splitting at $\nu = 2$). This model clearly does not capture the measured variation in v_{eff} . Far better results are found using the theory of Ref. [35], which accounts for many-particle contributions to CR in a single-mode approximation [44]. The fit has three parameters: an interaction-renormalized band velocity v^{ren} , the Dirac mass, and an overall Coulomb interaction that we fix at $V_C = \sqrt{\pi/2}e^2/(4\pi\epsilon l_B) = 50$ meV [45]. This fit provides a good account of the variation in v_{eff} vs T_i and also the size of the T_2 splittings, and it yields $v^{\text{ren}} = 1.105 \times 10^6$ m/s and $M = 2.76$ meV, close to the Dirac mass value at $\nu = 2$ discussed above. Carrying out this procedure at other magnetic fields and filling factors yields the v^{ren} values in Fig. 5(b). There, the resulting linear decrease against $\ln(\sqrt{B/B_0})$ is anticipated in Ref. [20], which predicts that the slope is given by $-(\alpha c/4e)$, where α is the fine-structure constant and c the speed of light. This running of the velocity with B is the generalization to finite field of the interaction-renormalized band velocity at zero field that was predicted before graphene was isolated [46] and seen in electronic transport [47]. The slope determines a dielectric constant of $\epsilon = 6.4$, which is likely dominated

by the in-plane ϵ of hexagonal boron nitride [48] and is in good agreement with magneto-Raman measurements [22].

F. Filling-factor dependence of T_2 and T_3

Finally, in Fig. 6, we explore the evolution of the second interband transition T_2 . Inspection of the color map and line cuts shows that a splitting is just resolved at $\nu = 0$, with peaks of approximately equal strength. This splitting evolves into a bright and sharp peak at $\nu = +1$ accompanied by a much weaker resonance on the high energy side; at $\nu = +2$, the splitting persists, but most of the spectral weight has shifted to the higher-energy peak. Similar to T_1 , at half-integer fillings, only a single broad resonance is seen, although the integrated intensity remains constant over this range of ν [30]. The peaks are split by 2.8 meV at $\nu = 0$ and 4.7 meV at $\nu = +2$. The behavior with changing magnetic field shown in Fig. 6(d) is rather different than for T_1 . For T_2 , a single $\nu = 0$ peak at 5 T gains a splitting at 8 T but reverts to a broader single resonance at 13 T. Since the T_2 transition comprises two nominally degenerate pairs of transitions $n = -2 \rightarrow +1$ and $-1 \rightarrow +2$ in each valley, as above, a weak valley coupling may split the degeneracy. Whether the splitting is observed may depend on the width of the resonances, which increases with field. For instance, at 8 T, the splitting is greater than the width, and it can be seen but is likely masked by further broadening of the resonance by 13 T. In contrast, at $\nu = 2$, the sharp single peak at 5 T evolves by 13 T into an unexpectedly large splitting, nearly 13 meV,

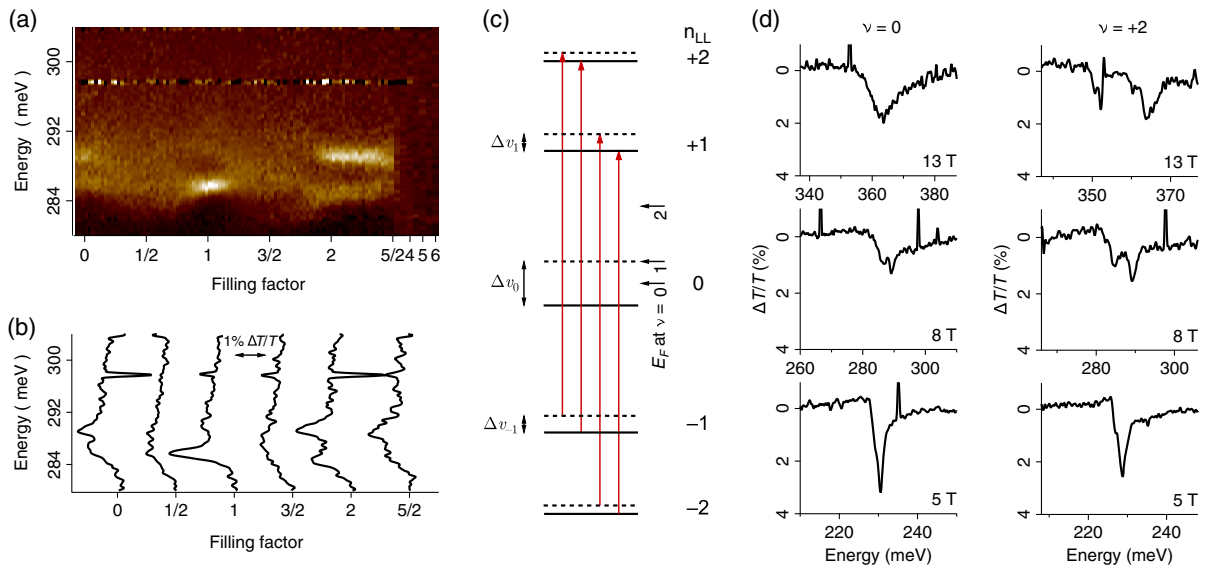


FIG. 6. Evolution of the second interband transition T_2 vs filling factor. (a) High-resolution map of T_2 for the same filling factor range as Fig. 1. The horizontal band at 298 meV is due to the harmonics of 60 Hz. Two peaks are just resolved at $\nu = 0$, while the spectrum is dominated by a single peak at $\nu = +1$, and two peaks appear again at $\nu = +2$, albeit with more intensity in the higher peak. The resonances are broader than those at T_1 and exhibit a high energy tail, which may be the result of multiple reflections in the substrate [25]. (b) Line cuts at half-integer filling factors. (c) Schematic of T_2 transitions, with the K (K') valley showing as a solid (dashed) line. Zeeman splittings are suppressed. (d) Spectra at $\nu = 0$ and $+2$ as a function of magnetic field. A remarkably large splitting, nearly 13 meV in size, appears at $\nu = +2$ at 13 T.

far larger than any other splitting seen in this work. In the many-particle theories of Refs. [19,35], interactions alone suffice to break the degeneracy of the $n = -2 \rightarrow +1$ and $-1 \rightarrow +2$ transitions at both $\nu = 0$ and 2; further, small corrections are expected for a finite Dirac mass. For T_2 , Ref. [35] predicts an approximately 3-meV splitting for a 5-meV gap. This prediction roughly matches the scale of splittings at 8 T but greatly underestimates the $\nu = 2$ splitting at 13 T. This large splitting is a surprise since, for $\nu = 2$, all orbital levels are filled or empty and interaction corrections should be minimal. At this time, no mechanism is clearly responsible for such a large splitting at $\nu = 2$.

The next higher interband transition T_3 also shows an intriguing and larger-than-expected sequence of splittings. A map of the transition energies vs filling factor, along with line cuts at an integer filling factor, is included in the Supplemental Material [30]. The signal-to-noise ratio in even-higher interband transitions is not sufficient to resolve splittings.

III. CONCLUSION

When applied to graphene, cyclotron resonance becomes a novel tool for spectroscopy of many-particle physics since Kohn's theorem no longer applies. Here, it enables us to follow the evolution of many-particle enhanced gaps in the broken-symmetry regime of clean monolayer graphene, where we find a Dirac mass that is significantly enhanced at half-filling of the zeroth LL, and Zeeman gaps both at and below the Fermi energy that are enhanced by direct or indirect exchange effects. These observations highlight the importance of lattice-scale interactions coupling the K and K' valleys in graphene. Moreover, a very small but finite particle-hole asymmetry is seen, which underscores the device quality and sets upper limits on the symmetry of the linear dispersion in graphene. These results promise that with continually improving device fabrication techniques, it will soon be possible to perform spectroscopy of excited states in the fractional quantum Hall regime.

We acknowledge informative discussions with H. Fertig, A. MacDonald, and K. Shizuya, and are grateful for support from the Institute of Materials Science and Engineering at Washington University in St. Louis. E. A. H. acknowledges partial support for this work under NSF CAREER DMR 1945278. K. W. and T. T. acknowledge support from the Elemental Strategy Initiative conducted by the MEXT, Japan, Grant No. JPMXP0112101001, JSPS KAKENHI Grants No. JP20H00354, and the CREST (JPMJCR15F3) JST.

[1] Y. Zhang, Z. Jiang, J. P. Small, M. Purewal, Y.-W. Tan, M. Fazlollahi, J. Chudow, J. Jaszczak, H. L. Stormer, and P.

- Kim, *Landau-Level Splitting in Graphene in High Magnetic Fields*, *Phys. Rev. Lett.* **96**, 136806 (2006).
- [2] J. Checkelsky, L. Li, and N. P. Ong, *Zero-Energy State in Graphene in a High Magnetic Field*, *Phys. Rev. Lett.* **100**, 206801 (2008).
- [3] Y. J. Song, A. F. Otte, Y. Kuk, Y. Hu, D. B. Torrance, P. N. First, W. A. de Heer, H. Min, S. Adam, M. D. Stiles, A. H. MacDonald, and J. A. Stroscio, *High-Resolution Tunnelling Spectroscopy of a Graphene Quartet*, *Nature (London)* **467**, 185 (2010).
- [4] A. F. Young, C. R. Dean, L. Wang, H. Ren, P. Cadden-Zimansky, K. Watanabe, T. Taniguchi, J. Hone, K. L. Shepard, and P. Kim, *Spin and Valley Quantum Hall Ferromagnetism in Graphene*, *Nat. Phys.* **8**, 550 (2012).
- [5] B. Hunt, J. D. Sanchez-Yamagishi, A. F. Young, M. Yankowitz, B. J. Leroy, K. Watanabe, T. Taniguchi, P. Moon, M. Koshino, P. Jarillo-Herrero, and R. C. Ashoori, *Massive Dirac Fermions and Hofstadter Butterfly in a van der Waals Heterostructure*, *Science* **340**, 1427 (2013).
- [6] A. A. Zibrov, E. M. Spanton, H. Zhou, C. Kometter, T. Taniguchi, K. Watanabe, and A. F. Young, *Even-Denominator Fractional Quantum Hall States at an Isospin Transition in Monolayer Graphene*, *Nat. Phys.* **14**, 930 (2018).
- [7] S.-Y. Li, Y. Zhang, L.-J. Yin, and L. He, *Scanning Tunneling Microscope Study of Quantum Hall Isospin Ferromagnetic States in the Zero Landau Level in a Graphene Monolayer*, *Phys. Rev. B* **100**, 085437 (2019).
- [8] Y. Jiang, Z. Lu, J. Gigliotti, A. Rustagi, L. Chen, C. Berger, W. de Heer, C. J. Stanton, D. Smirnov, and Z. Jiang, *Valley and Zeeman Splittings in Multilayer Epitaxial Graphene Revealed by Circular Polarization Resolved Magneto-infrared Spectroscopy*, *Nano Lett.* **19**, 7043 (2019).
- [9] M. Onodera, K. Kinoshita, R. Moriya, S. Masubuchi, K. Watanabe, T. Taniguchi, and T. Machida, *Cyclotron Resonance Study of Monolayer Graphene under Double Moiré Potentials*, *Nano Lett.* **20**, 4566 (2020).
- [10] P. Rao and I. Sodemann, *Cyclotron Resonance inside the Mott Gap: A fingerprint of Emergent Neutral Fermions*, *Phys. Rev. B* **100**, 155150 (2019).
- [11] Y. Shao, A. N. Rudenko, J. Hu, Z. Sun, Y. Zhu, S. Moon, A. J. Millis, S. Yuan, A. I. Lichtenstein, D. Smirnov, Z. Q. Mao, M. I. Katsnelson, and D. N. Basov, *Electronic Correlations in Nodal-Line Semimetals*, *Nat. Phys.* **16**, 636 (2020).
- [12] J. W. McClure, *Diamagnetism of Graphite*, *Phys. Rev.* **104**, 666 (1956).
- [13] V. P. Gusynin, S. G. Sharapov, and J. P. Carbotte, *Anomalous Absorption Line in the Magneto-Optical Response of Graphene*, *Phys. Rev. Lett.* **98**, 157402 (2007).
- [14] V. P. Gusynin, S. G. Sharapov, and J. P. Carbotte, *Unusual Microwave Response of Dirac Quasiparticles in Graphene*, *Phys. Rev. Lett.* **96**, 256802 (2006).
- [15] W. Kohn, *Cyclotron Resonance and de Haas-van Alphen Oscillations of an Interacting Electron Gas*, *Phys. Rev.* **123**, 1242 (1961).
- [16] C. Kallin and B. I. Halperin, *Many-Body Effects on the Cyclotron Resonance in a Two-Dimensional Electron Gas*, *Phys. Rev. B* **31**, 3635 (1985).
- [17] R. E. Throckmorton and S. D. Sarma, *Failure of Kohn's Theorem and the Apparent Failure of the f -Sum Rule in*

- Intrinsic Dirac-Weyl Materials in the Presence of a Filled Fermi Sea*, *Phys. Rev. B* **98**, 155112 (2018).
- [18] A. Iyengar, J. Wang, H. A. Fertig, and L. Brey, *Excitations from Filled Landau Levels in Graphene*, *Phys. Rev. B* **75**, 125430 (2007).
- [19] Y. A. Bychkov and G. Martinez, *Magnetoplasmon Excitations in Graphene for Filling Factors $\nu \leq 6$* , *Phys. Rev. B* **77**, 125417 (2008).
- [20] K. Shizuya, *Many-Body Corrections to Cyclotron Resonance in Monolayer and Bilayer Graphene*, *Phys. Rev. B* **81**, 075407 (2010).
- [21] R. Roldán, J.-N. Fuchs, and M. O. Goerbig, *Spin-Flip Excitations, Spin Waves, and Magnetoexcitons in Graphene Landau Levels at Integer Filling Factors*, *Phys. Rev. B* **82**, 205418 (2010).
- [22] C. Faugeras, S. Berciaud, P. Leszczynski, Y. Henni, K. Nogajewski, M. Orlita, T. Taniguchi, K. Watanabe, C. Forsythe, P. Kim, R. Jalil, A. K. Geim, D. M. Basko, and M. Potemski, *Landau Level Spectroscopy of Electron-Electron Interactions in Graphene*, *Phys. Rev. Lett.* **114**, 126804 (2015).
- [23] J. Sonntag, S. Reichardt, L. Wirtz, B. Beschoten, M. I. Katsnelson, F. Libisch, and C. Stampfer, *Impact of Many-Body Effects on Landau Levels in Graphene*, *Phys. Rev. Lett.* **120**, 187701 (2018).
- [24] Z. Jiang, E. A. Henriksen, L.-C. Tung, Y. J. Wang, M. E. Schwartz, M. Y. Han, P. Kim, and H. L. Stormer, *Infrared Spectroscopy of Landau Levels of Graphene*, *Phys. Rev. Lett.* **98**, 197403 (2007).
- [25] E. A. Henriksen, P. Cadden-Zimansky, Z. Jiang, Z. Q. Li, L.-C. Tung, M. E. Schwartz, M. Takita, Y. J. Wang, P. Kim, and H. L. Stormer, *Interaction-Induced Shift of the Cyclotron Resonance of Graphene Using Infrared Spectroscopy*, *Phys. Rev. Lett.* **104**, 067404 (2010).
- [26] Z.-G. Chen, Z. Shi, W. Yang, X. Lu, Y. Lai, H. Yan, F. Wang, G. Zhang, and Z. Li, *Observation of an Intrinsic Bandgap and Landau Level Renormalization in Graphene/Boron-Nitride Heterostructures*, *Nat. Commun.* **5**, 4461 (2014).
- [27] I. O. Nedoliuk, S. Hu, A. K. Geim, and A. B. Kuzmenko, *Colossal Infrared and Terahertz Magneto-optical Activity in a Two-Dimensional Dirac Material*, *Nat. Nanotechnol.* **14**, 756 (2019).
- [28] B. J. Russell, B. Zhou, T. Taniguchi, K. Watanabe, and E. A. Henriksen, *Many-Particle Effects in the Cyclotron Resonance of Encapsulated Monolayer Graphene*, *Phys. Rev. Lett.* **120**, 047401 (2018).
- [29] L. Wang, I. Meric, P. Y. Huang, Q. Gao, Y. Gao, H. Tran, T. Taniguchi, K. Watanabe, L. M. Campos, D. A. Muller, J. Guo, P. Kim, J. Hone, K. L. Shepard, and C. R. Dean, *One-Dimensional Electrical Contact to a Two-Dimensional Material*, *Science* **342**, 614 (2013).
- [30] See Supplemental Material at <http://link.aps.org/supplemental/10.1103/PhysRevX.10.041006> for discussion of infrared normalization, additional absorption features, linewidths, sample temperature, signal intensity, additional linecuts for T_1 , T_2 , and T_3 vs filling factor and magnetic field, the method for extracting gap energies, and additional electronic transport data.
- [31] C. R. Dean, A. F. Young, I. Meric, C. Lee, L. Wang, S. Sorgenfrei, K. Watanabe, T. Taniguchi, P. Kim, K. L. Shepard, and J. Hone, *Boron Nitride Substrates for High-Quality Graphene Electronics*, *Nat. Nanotechnol.* **5**, 722 (2010).
- [32] A. A. Zibrov, C. Kometter, H. Zhou, E. M. Spanton, T. Taniguchi, K. Watanabe, M. P. Zaletel, and A. F. Young, *Tunable Interacting Composite Fermion Phases in a Half-Filled Bilayer-Graphene Landau Level*, *Nature (London)* **549**, 360 (2017).
- [33] P. T. Coleridge, R. Stoner, and R. Fletcher, *Low-Field Transport Coefficients in GaAs/Ga_{1-x}Al_xAs Heterostructures*, *Phys. Rev. B* **39**, 1120 (1989).
- [34] S. Syed, M. J. Manfra, Y. J. Wang, R. J. Molnar, and H. L. Stormer, *Electron Scattering in AlGaN/GaN Structures*, *Appl. Phys. Lett.* **84**, 1507 (2004).
- [35] K. Shizuya, *Many-Body Effects on Landau-Level Spectra and Cyclotron Resonance in Graphene*, *Phys. Rev. B* **98**, 115419 (2018).
- [36] A. A. Sokolik and Y. E. Lozovik, *Many-Body Filling Factor Dependent Renormalization of Fermi Velocity in Graphene in Strong Magnetic Field*, *Phys. Rev. B* **99**, 085423 (2019).
- [37] O. Dial, R. C. Ashoori, L. N. Pfeiffer, and K. W. West, *High-Resolution Spectroscopy of Two-Dimensional Electron Systems*, *Nature (London)* **448**, 176 (2007).
- [38] M. Kharitonov, *Phase Diagram for the $\nu = 0$ Quantum Hall State in Monolayer Graphene*, *Phys. Rev. B* **85**, 155439 (2012).
- [39] H.-K. Tang, J. N. Leaw, J. N. B. Rodrigues, I. F. Herbut, P. Sengupta, F. F. Assaad, and S. Adam, *The Role of Electron-Electron Interactions in Two-Dimensional Dirac Fermions*, *Science* **361**, 570 (2018).
- [40] N. M. R. Peres, F. Guinea, and A. H. C. Neto, *Electronic Properties of Disordered Two-Dimensional Carbon*, *Phys. Rev. B* **73**, 125411 (2006).
- [41] P. Plochocka, C. Faugeras, M. Orlita, M. L. Sadowski, G. Martinez, M. Potemski, M. O. Goerbig, J.-N. Fuchs, C. Berger, and W. A. de Heer, *High-Energy Limit of Massless Dirac Fermions in Multilayer Graphene using Magneto-Optical Transmission Spectroscopy*, *Phys. Rev. Lett.* **100**, 087401 (2008).
- [42] R. S. Deacon, K.-C. Chuang, R. J. Nicholas, K. S. Novoselov, and A. K. Geim, *Cyclotron Resonance Study of the Electron and Hole Velocity in Graphene Monolayers*, *Phys. Rev. B* **76**, 081406 (2007).
- [43] D. Nakamura, H. Saito, H. Hibino, K. Asano, and S. Takeyama, *Quantum Limit Cyclotron Resonance in Monolayer Epitaxial Graphene in Magnetic Fields up to 560 T: The Relativistic Electron and Hole Asymmetry*, *Phys. Rev. B* **101**, 115420 (2020).
- [44] A. H. MacDonald, H. C. A. Oji, and S. M. Girvin, *Magnetoplasmon Excitations from Partially Filled Landau Levels in Two Dimensions*, *Phys. Rev. Lett.* **55**, 2208 (1985).
- [45] The curve fits are not sensitive to the precise value of V_C . Specifically, changing the value of ϵ in V_C results in different values of v^{ren} returned by the fits in Fig. 5(a); but the slope of the new v^{ren} vs $\ln(l_{B_0}/l_B)$ is unchanged. In other words, the relative variation of the measured v_{eff} at different fields has physical meaning independent of the

- particular renormalization employed, as discussed in Refs. [20,35].
- [46] J. Gonzalez, F. Guinea, and M. Vozmediano, *Non-Fermi Liquid Behavior of Electrons in the Half-Filled Honeycomb Lattice (A Renormalization Group Approach)*, *Nucl. Phys.* **B424**, 595 (1994).
- [47] D. C. Elias, R. V. Gorbachev, A. S. Mayorov, S. V. Morozov, A. A. Zhukov, P. Blake, L. A. Ponomarenko, I. V. Grigorieva, K. S. Novoselov, F. Guinea, and A. K. Geim, *Dirac Cones Reshaped by Interaction Effects in Suspended Graphene*, *Nat. Phys.* **7**, 701 (2011).
- [48] A. Laturia, M. L. Van de Put, and W. G. Vandenberghe, *Dielectric Properties of Hexagonal Boron Nitride and Transition Metal Dichalcogenides: From Monolayer to Bulk*, *npj 2D Mater. Appl.* **2**, 6 (2018).